Showcasing research from the Femtosecond Laser Labs in the Department of Chemistry and the Center for Lasers and Photonics at the Indian Institute of Technology Kanpur, India

Title: Precise control and measurement of solid−liquid interfacial temperature and viscosity using dual-beam femtosecond optical tweezers in the condensed phase

This paper reports a novel method of microrheology based on femtosecond optical tweezers, which in turn enables a direct measure and control of *in situ* temperature at microscale volumes. A polystyrene bead trapped with noninvasive pulsed 780 nm laser responds spontaneously to changes in its environment induced by a co-propagating 1560 nm pulsed heating laser. ''Hot Brownian motion'' of the trapped bead is reflected in the corner frequency as deduced from its power spectrum. Changes in corner frequency values enable calculation of viscosity and temperature at the solid−liquid interface.

ROYAL SOCIETY OF CHEMISTRY

www.rsc.org/pccp

PAPER

Precise control and measurement of solid–liquid interfacial temperature and viscosity using dual-beam femtosecond optical tweezers in the condensed phase†

Dipankar Mondal,[a] Paresh Mathur[b] and Debabrata Goswami*[ab]

We present a novel method of microrheology based on femtosecond optical tweezers, which in turn enables us to directly measure and control *in situ* temperature at microscale volumes at the solid–liquid interface. A noninvasive pulsed 780 nm trapped bead spontaneously responds to changes in its environment induced by a co-propagating 1560 nm pulsed laser due to mutual energy transfer between the solvent molecules and the trapped bead. Strong absorption of the hydroxyl group by the 1560 nm laser creates local heating in individual and binary mixtures of water and alcohols. "Hot Brownian motion" of the trapped polystyrene bead is reflected in the corner frequency deduced from the power spectrum. Changes in corner frequency values enable us to calculate the viscosity as well as temperature at the solid–liquid interface. We show that these experimental results can also be theoretically ratified.

1. Introduction

Optical tweezers[1,2] are being used in various fields of research for numerous applications. The principle of optical trapping is based on radiation pressure exerted by light and is mainly used to hold and manipulate various objects with sizes ranging from several nanometers to a few microns. We use 780 nm femtosecond pulsed optical tweezers[3–5] that provide a high gradient force from only 7 mW average laser power. Such a high peak-power Gaussian laser beam can easily trap and manipulate small microparticles, nanoparticles or even quantum dots.[6] This trapping wavelength is transparent through water, alcohol, most of the bio-molecule solutions, cells, and is confirmed to be safe and non-invasive due to its very low absorption coefficient.[7] Consequently, the temperature rise is negligible for the low laser powers used in such experiments. On the other hand, there is significant evidence of temperature rise for a 1560 nm pulsed laser because of the strong absorption coefficient at the $\nu_1 + \nu_3$ combination band (*i.e.*, two fundamental vibrational bands are simultaneously excited).[8–10] The vibrational combination band near 1560 nm of hydroxyl, amine and thiol can also be useful for investigating viscosity changes from the temperature rise. Earlier, stable 3D trapping of cells, viruses, bacteria, *etc.* has

been demonstrated at a 1064 nm continuous wave (cw) laser with low absorption under experimental conditions.[11–14] However, the effects on biological systems due to high power 1064 nm absorption arising from the vibrational combination band $(2\nu_2 + \nu_3)$[15,16] of water have also remained a subject of interest. Thus, the possibility of using a single beam laser trap to simultaneously measure thermal effects has its shortcomings.

We have instead devised a two-colour approach, which in contrast uses one laser at 1560 nm as an independent source of temperature control that is being simultaneously detected by another co-propagating stable laser trap at 780 nm. The co-propagated non-invasive trapping laser at 780 nm probes the effect of the pulsed 1560 nm laser. The main uniqueness of this work over already existing methods[17–19] lies in the use of a femtosecond optical trap and a heating laser rather than cw lasers, as well as in the inclusion of a correction term for the temperature change. The effects of surroundings on bio-systems have often impacted the efficiencies of their physical activities. In this regard, viscosity (η) and temperature (T) are two such physical parameters that have a strong control on the nature of bio-molecular activity.[20–25]

We probe the Brownian motion[26,27] of a spherical polystyrene bead suspended in condensed media. Due to Brownian motion, there exists a characteristic frequency of the trapped particle for every trapping laser power, beyond which the particle cannot remain trapped. This characteristic frequency is known as the corner frequency. Our main focus from the newly developed technique is to measure the corner frequency at different heating laser powers, wherein the spherical polystyrene bead

[a] *Indian Institute of Technology Kanpur, Department of Chemistry, Kanpur 208016, Uttar Pradesh, India. E-mail: dgoswami@iitk.ac.in*

[b] *Indian Institute of Technology Kanpur, Center for Lasers and Photonics, Kanpur 208016, Uttar Pradesh, India*

† Electronic supplementary information (ESI) available. See DOI: 10.1039/c6cp03093a

This journal is © the Owner Societies 2016

Phys. Chem. Chem. Phys., 2016, **18**, 25823–25830 | 25823

spontaneously equilibrates itself to the surrounding temperature. The nature of Brownian motion can be understood by the theory developed by Einstein.[28] The energy transfer occurs between the trapped bead and the solvents resulting in the transformation of thermal energy of solvents into the kinetic energy of the trap bead. Thus the hot solvent molecules resulting from 1560 nm absorption can continuously dissipate heat to the trapped stationary bead which will be reflected in the frequency spectrum of Brownian noise exhibited by the bead. The stochastic motion[29] of a spherical bead confined in harmonic trapping potential under a Gaussian laser pulse having thermal molecular motion will give rise to diffusion, which increases with temperature. Interestingly, the simultaneous increase of the diffusion coefficient and corner frequency will keep the net trap stiffness constant. However, the distinct nature of individual trapped particles may provide an independent measure that would elucidate the absolute instantaneous temperature rise at the trapped bead surface–solvent layer. Temperature dependence of viscosity enables us to phenomenologically solve the expression of nonlinear equation for binary liquid mixtures using numerical methods. Our microrheological[30–33] investigations on the temperature and viscosity of individual and binary solvent media of water and alcohols can be used to map the environmental temperature or viscosity[34] at the solid–liquid interface around the confined space of the micro to nano size regime.

This contactless temperature measurement in the sub-microscale volume also leads to the inception of a new micro-viscometer, which can be used to probe the physical properties of confined systems and the effect of surrounding on their behaviour.[35] Furthermore, we can apply our method to elucidate the structural responses of trapped protein macromolecules[36] in different solvents and at different temperatures.

Here we demonstrate the measure of local temperature as well as viscosity in water–methanol and water–ethanol binary mixtures both theoretically and experimentally. Our initial model was based only on conduction;[9,37] thereafter, we observed a deviation between the calculated and experimental data towards higher temperatures.[38,39] We show here that it is possible to match the experimental results better with a modified model for such liquid mixtures, when we take advantage of our pure sample data. The observed deviation in water has helped us to introduce a new correction term in the theoretical model. With this approach, our method can be extended to any complex fluid media of solvent mixtures having N–H, S–H, O=C–O–H, and P–H groups.

2. Methods and materials

In our optical tweezers setup (Fig. 1), the laser source used is an Er-doped fibre laser (Femtolite C-20-SP, IMRA Inc., USA), which generates femtosecond laser pulses centred at fundamental 1560 nm wavelength and at its second harmonic 780 nm with pulse-widths 300 fs and 100 fs, respectively. The two laser pulse outputs are collinear at a repetition rate of 50 MHz. A commercial oil immersion objective (UPlanSApo, 100×, 1.4 NA, OLYMPUS Inc., Japan) was
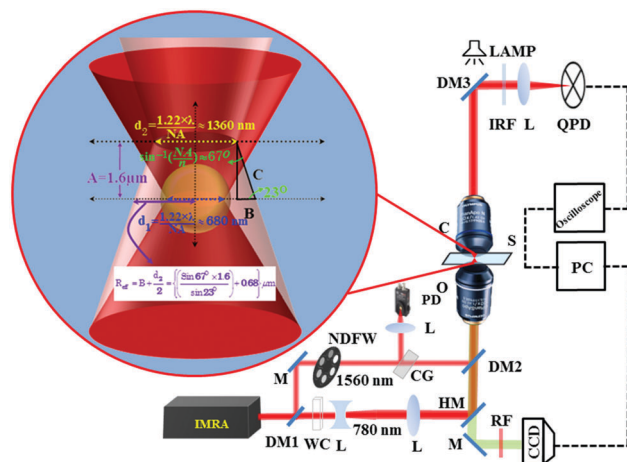

Fig. 1 Optical setup with labels: DM (1–3): dichroic mirror; M: mirror; CG: cover glass; NDFW: neutral density filter wheels; L: lens; PD: photodiode; WC: water cuvette; HM: hot mirror; O: objective lens; S: sample chamber; C: condenser lens; IRF: infrared filter; RF: red filter; QPD: quadrant photodiode; CCD: camera (charge coupled device). Ray optics diagram (inset) (see S1, ESI†).

used to achieve tight focusing; simultaneously the forward scattered light was collected with another oil immersion objective (60×, PlanApo N, 1.42 NA, OLYMPUS Inc., Japan) and focused onto a quadrant photodiode (QPD) (2901, Newport Co., USA). The QPD output was connected to a digital oscilloscope (Waverunner 64Xi, LeCroy, USA) interfaced with a personal computer through a GPIB card (National Instruments, USA). Data were acquired using the LabVIEW program. Spectroscopic grade methanol (MeOH) and ethanol (EtOH) were purchased from Merck, India, and were used without any further purification. We used a 500 nm mean radius (T8883, Life Technology, USA) fluorophore coated polystyrene sphere suspended in H_2O–MeOH and H_2O–EtOH mixtures. The commercially available polystyrene nanosphere solution (T8883: concentration 3.6×10^{10} particles per ml) was diluted to nano-molar concentration and well sonicated for immediate use in trapping experiments. The video of the trapping events was monitored using a CCD camera (350 K pixel, e-Marks Inc., USA). White light was used for bright field illumination. Trapping laser power was measured using a power meter (FieldMate, Coherent, USA) as well as a silicon amplified photodiode (PDA100A-EC, Thorlabs, USA) and 1560 nm power was measured using a calibrated biased InGaAs detector (DET10C/M, Thorlabs, USA). All laser power measurements with the power-meter were made just before the sample chamber. The absorption spectrum was collected using an absorption spectrometer (Lambda 900, PerkinElmer, USA). A linear motorized stage (UE1724SR driven by ESP300, Newport Co., USA) was used, which was interfaced with a personal computer through the GPIB card. We used a mechanical shutter (SR475), controlled through LABVIEW programming, operating at the maximum rate of 100 kHz to result in an opening time that is shorter than or comparable to the thermal relaxation time. The thermal relaxation time is defined as the average time required to achieve maximum

25824 | Phys. Chem. Chem. Phys., 2016, 18, 25823–25830

This journal is © the Owner Societies 2016

temperature at the surface of the bead.[40] The entire experiment has been done twice to ensure that at least 10 data points are averaged for each time.

3. Results and discussion

3.1 Theoretical section

When two different colour light beams are focused by the same objective they do not focus at the same plane. Our proposed model (see S1, ESI†) is able to calculate the effective fluence of the 1560 nm pulse laser at the focus of the 780 nm laser, where the polystyrene particle is trapped. This new approach overcomes the difficulty of two different colour pulsed laser fluence calculation of any desired plane though they focus at different positions with 1.6 μm separation when focused by the same objective as shown in the Experimental section (Fig. 1). We measured this distance between two colour focal points by placing a thin cover slip sample chamber containing 10^{-4} M Rhodamine-6G in water. The maximum two photon fluorescence (TPF) is emitted from the focal plane of the 780 nm laser. This epifluorescence is measured on a CCD at the back focal plane (Fig. 1). When the illuminated sample is moved with respect to the 780 nm focal plane with a linear motorized stage (of minimum resolution 0.00001 mm), the minimum transmittance signal occurs on the InGaAs 1560 nm detector at a position 1.6 μm further, which is the focal plane of 1560 nm. For this calibration measurement, we placed an aperture just before the InGaAs detector, which replaces DM3 in Fig. 1. Using the "Law of sines",[41] the fluence of the 1560 nm pulsed laser at the focus of 780 nm trapping laser can be calculated by the following equation (see S1, ESI†):

$$F_0 = \frac{\text{Pulse energy}}{\pi \left[\left\{ \left(\frac{\sin 67°}{\sin 23°} \times 1.6 \right) + 0.68 \right\} \times 10^{-6} \right]^2} \quad (1)$$

The half angle of the objective does not change since the focal length of the $100\times$ objective is higher (above 100 times) than the separation between the two focal points of two colours (Fig. 1). We have thus effectively used the geometric model as a reasonable approximation. The half angle of the cone formed by the focusing laser beam is ~67° calculated from the relation NA = $n\sin\alpha$, using 1.4 numerical aperture (NA) of the objective lens and a refractive index (n) of 1.52 for the immersion oil. Using the formula[42] focal spot = $(1.22 \times \lambda)/$NA, where λ is the laser wavelength, we calculate the beam waist of 780 nm and 1560 nm lasers at focus as 680 nm and 1360 nm respectively. The increase in temperature with respect to room temperature (T_0) due to the absorption of a 1560 nm Gaussian beam by solvent media can be evaluated using the following equation:[43]

$$T_{\max} - T_0 = 0.783 \frac{F}{\tau_p} \frac{2\sqrt{\tau_p}}{\sqrt{\pi K \rho C}} \quad (2)$$

The total fluence (F) absorbed by solvents used is calculated from $F = A \times (1 - |r_f|^2)F_0$, where F_0 is the laser fluence before the sample chamber and r_f is the reflection coefficient, which is

Table 1 The used physical parameters of the trapping solvent

Sample	Density (ρ) (kg m^{-3})	Heat capacity (C) (J kg^{-1} K^{-1})	Thermal conductivity (κ) (W K^{-1} m^{-1})	Absorbance (A)
H$_2$O	997[a]	4180[c]	0.600[e]	
MeOH	786[b]	2250[d]	0.206[e]	
EtOH	785[b]	2440[c]	0.178[e]	
H$_2$O–EtOH mixture	990	4120	0.586	0.113
H$_2$O–MeOH mixture	987	4090	0.581	0.117

[a] From ref. 44. [b] From ref. 45. [c] From ref. 46. [d] From ref. 47. [e] From ref. 48.

calculated from the cover glass refractive index, n, using the relation $r_f = \left| \frac{n-1}{n+1} \right|$. "$A$" is the measured absorbance of binary mixtures in the thin sample chamber. The other parameters used in eqn (2) (see S2, ESI†) are density (ρ), thermal conductivity (κ), and heat capacity (C) for binary mixtures that can be calculated from the following set of equations, using pure component physical parameters (Table 1):[44–48]

$$\left. \begin{array}{l} \rho_{\text{mix}} = \sum_{i=1}^{j} X_i \rho_i \\[2mm] \kappa_{\text{mix}} = \sum_{i=1}^{j} X_i \kappa_i \\[2mm] C_{\text{mix}} = \sum_{i=1}^{j} X_i C_i \end{array} \right\} \quad (3)$$

In eqn (3) the index j is 2 for binary mixtures, whereas the index i represents the pure component of binary mixtures. The mole fraction (X) is calculated from the volume fraction (φ) and molecular weight (M) and density (ρ). We note that use of such an ideal behaviour is impractical for viscosity, which is dependent on intermolecular interactions. The viscosity of binary mixtures is calculated based on the temperature rise (Tables 2 and 3) using the following equations:[49–51]

$$\ln \eta_{\text{binary mix}} = \varphi_1 \ln \eta_1 + \varphi_2 \ln \eta_2 + \Delta \ln \eta^{\text{excess}} \quad (4)$$

$$\eta_{\text{binary mix}} = \exp \left\{ \left(0.9 \times \ln \left(2.414 \times 10^{-2} \times 10^{\frac{247.8}{140-T}} \right) \right) + \left(0.1 \times \left(A_i + \frac{B_i}{C_i + T} \right) \right) + \Delta \ln \eta^{\text{excess}} \right\} \quad (5)$$

Here $\Delta\ln(\eta^{\text{excess}})$ is the excess viscosity due to mixing, which is calculated by using the method developed by Wolf et al.[52,53] For each individual alcohol, A, B and C are Vogel's equation parameters (see S3, ESI†).

3.2 Experimental section

We have used a pulsed laser at 780 nm with 7 mW of average power to trap the polystyrene bead of 500 nm mean radius. The solvent media used are H$_2$O–EtOH and H$_2$O–MeOH mixtures. In both the cases, a volume ratio of 90 : 10 is used. The trapping laser can be considered non-invasive due to very low absorption
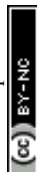
Table 2 Theoretical and experimental data for a 90 : 10 (volume-wise) H_2O–EtOH mixture

1560 nm Power (µW)	Corner frequency (Hz)	Fluence (J m^{-2})	Theoretical data					Experimental data	
			$T_{max} - T_0$ (K)	Viscosity (Pa s) $\times 10^{-3}$	Corrected ΔT_{theo}	Corrected viscosity (Pa s) $\times 10^{-3}$		Temperature rise (K)	Viscosity (Pa s) $\times 10^{-3}$
0	83	0	0	1.60	0	1.60		0	1.60
209	88	0.0672	7.6	1.32	5.5	1.35		2.2	1.51
363	96	0.1167	13.2	1.23	9.6	1.29		6.1	1.38
420	110	0.1351	15.3	1.19	11.1	1.25		12.5	1.20
630	119	0.2026	22.9	1.10	16.6	1.18		16.2	1.11
830	133	0.2669	30.2	1.02	21.9	1.10		21.5	0.99

Table 3 Theoretical and experimental data for a 90 : 10 (volume-wise) H_2O–MeOH mixture

1560 nm Power (µW)	Corner frequency (Hz)	Fluence (J m^{-2})	Theoretical data					Experimental data	
			$T_{max} - T_0$ (K)	Viscosity (Pa s) $\times 10^{-3}$	Corrected ΔT_{theo}	Corrected viscosity (Pa s) $\times 10^{-3}$		Temperature rise (K)	Viscosity (Pa s) $\times 10^{-3}$
0	106	0	0	1.30	0	1.30		0	1.30
170	116	0.0547	6.5	1.14	4.8	1.18		3.9	1.19
266	122	0.0855	10.1	1.10	7.4	1.14		6.2	1.13
363	129	0.1167	13.8	1.05	10.2	1.10		8.8	1.07
460	137	0.1479	17.5	1.00	12.9	1.06		11.5	1.01
630	143	0.2026	23.9	0.93	17.6	1.00		14.0	0.96
763	150	0.2454	29.0	0.88	21.4	0.96		16.1	0.92

coefficients of the solvents used.[7] Simultaneously, we also irradiated our trapped volume by a 1560 nm IR laser where binary solvents have high absorption coefficients resulting in local heating around the trapped particle. The beam waist spot size of the trapping laser is 680 nm and that of the heating laser is 1360 nm whereas the effective heating beam radius at the trapping plane is out of the Rayleigh range[54] ($\pi \omega_0^2/\lambda$ = 931 nm) as the separation is 1.6 µm (see Theoretical section for details). Due to the temperature rise, the trapped 500 nm mean radius particle will show a different behaviour, which is reflected in its "Hot Brownian motion".[55–57] We measure the temperature change between the polystyrene bead surface and the surrounding liquid layer (through the corner frequency shift) to indicate that thermal flow exists, and the bead displacement due to this flow is coupled with that of a regular confined Brownian motion. We only correlate the measured displacement of the confined Brownian motion as long as our temperature change is not very large according to our model. We have thus probed the confined Brownian motion of the polystyrene bead trapped in a harmonic potential[58] generated by a Gaussian laser pulse, which can be described by the Langevin equation[59]

$$m\ddot{X}(t) + \gamma \dot{x}(t) + \kappa_{TS}x(t) = \zeta_{therm}(t) \tag{6}$$

where m denotes the particle mass, x signifies the time dependent position, γ is the viscous drag coefficient as per Stokes' law, κ_{TS} is the spring constant (or trap stiffness) and ζ_{therm} is the time dependent random force. By solving the above equation, we can fit our experimental one-sided power spectrum. Typically, in the power spectrum, power is measured in the interval f and $f + df$, which does not distinguish between $+f$ and $-f$. In such cases, it is possible to define one-sided

power spectral density[60] (PSD) (see S4, ESI†) by the following Lorentzian:[61]

$$p_x(f) = \left\langle p_x(f)^{(exp)} \right\rangle = \frac{A}{(f_c^2 + f^2)} = \frac{D}{\pi^2(f_c^2 + f^2)} \tag{7}$$

Here A is a fitting parameter which has information about D, the diffusion coefficient. "A" has the unit V^2 s^{-1}. The diffusion coefficient can be evaluated from A using the voltage to position calibration[62,63] factor. We have analysed the forward scattered data of the trapped bead that have been collected with a QPD at a sampling rate of 20 kHz for the first 2.5 seconds of trapping. This is to minimize the convection effects. The acquired data of channels X and Y are de-correlated by removing the cross-talk[61,64] between them. The processed data are then fitted with eqn (7) to obtain the respective corner frequency within different solvents and at different 1560 nm laser heating powers.

We observed an increasing trend in the corner frequency (f_C), which is deduced from the power spectrum (Fig. 2a and b), with an increase in 1560 nm laser power. From our theoretical model (see eqn (2)), we notice that there is a linear relationship between 1560 nm laser power and the corresponding temperature rise. Simultaneously, from eqn (4) and (5), we note that viscosity decreases with an increase in 1560 nm power. Within our experimental range, when the viscosity change with respect to the temperature change lies in the linear regime, we have considered the trap stiffness ($\kappa = 2\pi f_C \gamma$) as a constant parameter. This statement is correct as long as there is a continuous change in viscosity with the heating laser source for a constant-sized trapped particle in the same solvent medium (see S5, ESI†). This has enabled us to measure (Tables 2 and 3) the viscosity change and the temperature rise around the interface of the trapped bead and the surrounding solvent molecules from
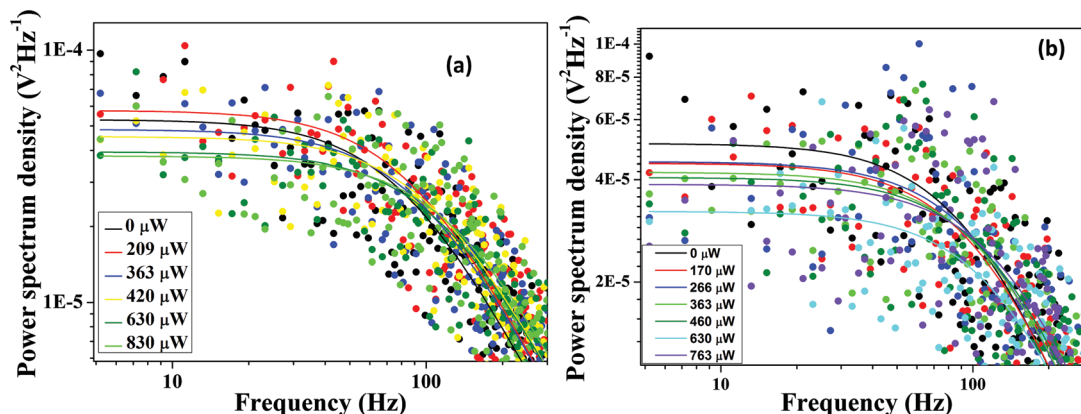
Fig. 2 Experimentally measured power spectrum (scatter points) and the respective Lorentzian fitted data (solid line) for a 500 nm radius fluorophore coated polystyrene bead in the (a) water–ethanol mixture and (b) water–methanol mixture.

the formula $\eta \cdot f_C$ = constant.[19,65] All our experimental measurements are performed with respect to the room temperature viscosity at the corresponding corner frequency in individual binary solvents when the 1560 nm laser is absent.

Experimentally, we first observe the corner frequency change, which allows us to calculate the viscosity around the trapped bead. From our experimentally measured viscosity, we calculate the temperature rise of the respective binary mixtures (Tables 2 and 3) by rearranging the variables in eqn (5) and solving with MATLAB®. The particle experiencing viscous drag, $\gamma = 6\pi\eta r$ (r = 500 nm), has trap stiffness, κ_{TS}, for H_2O–EtOH and H_2O–MeOH binary mixtures as 0.0078 ± 0.0002 pN nm^{-1} and 0.0081 ± 0.0002 pN nm^{-1} respectively. The confidence range of our trap stiffness (see S5, ESI†) results is obtained by the standard deviation of all stiffness measurements at different temperatures. As expected, viscosity changes around the trapped bead with respect to temperature changes are linear (Fig. 3a). Our experimental data in Tables 2 and 3 show that the temperature rise between the theoretical calculation and the experimental measurement deviates with the increase in temperature, which is also true for viscosity. This is due to the fact that besides conduction, convection also plays an important role in heat transfer towards high temperature, since with temperature rise, the focal plane separation changes. The refractive index changes as a result of the diverging optical lens[66]

formed in solvent media with the increase in temperature at the focal volume. Additionally, due to the high NA objective, there could be a critical angle effect, which could consistently result in an overestimation of our theoretically estimated temperature change. Consequently, the separation of focal points for the two laser wavelengths becomes slightly more, which reduces the temperature at the focal volume around the optical trap and this is reflected in our experimental results. To account for this, we add a correction term to eqn (2) from our earlier study (see S6, ESI†) and generalize it for use in binary mixtures:

$$T_{\max} - T_0 = 0.783\frac{F}{\tau_p}\frac{2\sqrt{\tau_p}}{\sqrt{\pi K \rho C}} - \left\{ x_1 \left[\left(\frac{dT}{dP}\right)_{\text{Theo}} - \left(\frac{dT}{dP}\right)_{\text{Exp}} \right]_{C1} \right.$$
$$\left. + (1 - x_1)\left[\left(\frac{dT}{dP}\right)_{\text{Theo}} - \left(\frac{dT}{dP}\right)_{\text{Exp}} \right]_{C2} \right\} \times P_{\text{avg}}$$
(8)

Since water is the dominant species in our particular experiments, we can simplify eqn (8) further as follows:

$$T_{\max} - T_0 = 0.783\frac{F}{\tau_p}\frac{2\sqrt{\tau_p}}{\sqrt{\pi K \rho C}} - \left[\left(\frac{dT}{dP}\right)_{\text{Theo}} - \left(\frac{dT}{dP}\right)_{\text{Exp}} \right]_{C1} \times P_{\text{avg}}$$
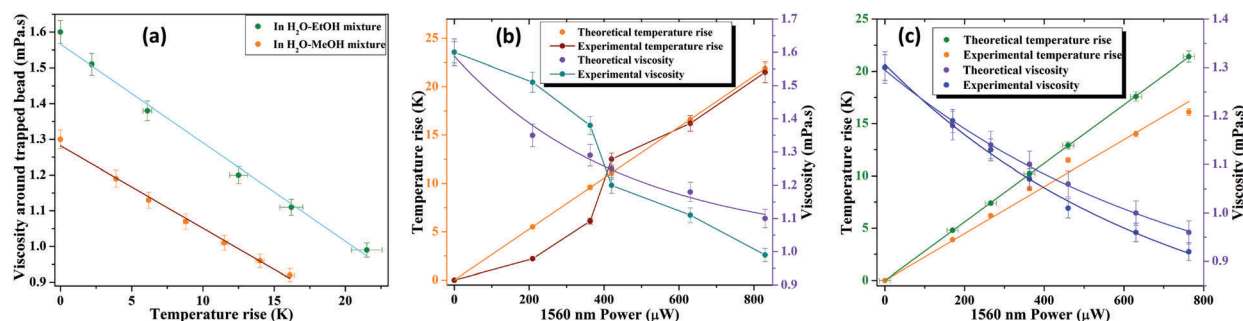(8a)

Fig. 3 (a) Experimental data for viscosity *versus* temperature rise (scatter plot) around the trapped bead and the corresponding linear fitting (solid line). The comparison of our theoretically corrected data for temperature rise (left side *Y* axis) and viscosity (right side *Y* axis) with experimental data in the respective (b) water–ethanol mixture and (c) water–methanol mixture.

This journal is © the Owner Societies 2016

Phys. Chem. Chem. Phys., 2016, **18**, 25823–25830 | 25827

Here C1 represents pure water while the other parameters are the same as explained in the Theoretical section. In pure water, the theoretical gradient of temperature rise, calculated from eqn (2), is $(dT/dP)_{Theo} = 0.034$ K μW^{-1}, while the measured experimental gradient of temperature rise is $(dT/dP)_{Exp} = 0.024$ K μW^{-1}. The correction term introduced is the difference of these two values for binary solvent mixtures in eqn (8a). We plot the corrected theoretical temperature rise and the corresponding viscosity in Fig. 3b and c for H_2O–EtOH and H_2O–MeOH respectively and compare them to the corresponding experimental data (also presented in Tables 2 and 3). For theoretical calculations, we first estimated the temperature rise ($T_{max} - T_0$ (K)) from applied 1560 nm pulse laser fluence using eqn (2), which is converted *via* eqn (5) to measure the surrounding viscosity. The corrected ΔT_{theo} is evaluated from eqn (8a), which is again transformed to measure the corrected viscosity using eqn (5).

It is important to note from Fig. 3b that we observed a very unusual experimental behaviour of temperature rise (ΔT) and viscosity (η) in the H_2O–EtOH binary mixture. This is in spite of the fact that the theoretical temperature rise (ΔT) followed a linear increase with 1560 nm laser power, and the viscosity (η) followed the Vogel equation. This unusual behaviour is due to the loss of the individual properties of the constituent liquids in the binary mixtures, which is better explained in terms of non-ideal behaviour of the binary mixture as presented in Fig. 4. Fig. 4a shows the comparative plot of the slope of $1/f_C$ with 1560 nm laser power for water with methanol as well as ethanol. The distinct behaviour of the nature of the trap is

Fig. 4 (a) Comparative plot of inverse corner frequency *versus* power of a 1560 nm femtosecond laser with linear fitting (solid line) of water with pure MeOH and pure EtOH. (b) The comparison between excess heat capacity of H_2O–MeOH (black line) and H_2O–EtOH (red line) binary mixtures at 25 °C.

evident from the distinct slopes in Fig. 4a for the three pure liquids, *i.e.*, water (−2.95), methanol (−5.71) and ethanol (2.06), which also conform to the trend in the respective viscosities (η) of these pure liquids ($\eta_{EtOH} > \eta_{H_2O} > \eta_{MeOH}$). These numbers are indicative of the fact that the intermolecular forces in pure water and in pure ethanol are more similar as compared to the intermolecular forces in pure methanol. This would mean that in the case of binary mixtures of water with ethanol or methanol, the water–ethanol mixture would overall have more intermolecular force as compared to that of water–methanol. To further ratify our conjecture obtained from Fig. 4a, we plotted the comparative excess heat capacity in Fig. 4b, which shows that for a 10% volume mixture of H_2O–MeOH and H_2O–EtOH, the excess heat capacity, $C_{p,mix}^{E}$, of the water–ethanol mixture (6.69 J K^{-1} mol^{-1}) is higher than that of the water–methanol mixture (1.74 J K^{-1} mol^{-1}).

Since excess heat capacity is the measure of deviation from the ideal nature of mixtures, water–ethanol shows a higher deviation from ideal behaviour as compared to water–methanol. This corresponds to our observation from Fig. 3 that the water–methanol mixture follows the expected trend of 1560 nm laser heating while the water–ethanol mixture shows deviation.

The isobaric molar heat capacity of the binary mixture can be expressed by eqn (9) and (10). Thus, the excess heat capacity can be calculated by using eqn (11):[67]

$$\left(\frac{\partial H_{m,mix}}{\partial T}\right)_p = X_{C1}\left(\frac{\partial H_{m,C1}}{\partial T}\right)_p + X_{C2}\left(\frac{\partial H_{m,C2}}{\partial T}\right)_p + \left(\frac{\partial H_m^E}{\partial T}\right)_p \tag{9}$$

$$C_{p,m,mix} = X_{C1}C_{p,C1} + X_{C2}C_{p,C2} + C_{p,mix}^{E} \tag{10}$$

$$C_{p,mix}^{E} = \phi(1-\phi)\sum_{i=1}^{n} a(1-2\phi)^{i-1} \tag{11}$$

where C2 represents the second component of the binary mixture with water, H is the enthalpy, φ is the volume fraction of water and the "a" value is used from ref. 67.

Thus, our experimental results follow our theoretical framework that we have developed for the measurement of sub-micron volume temperatures as well as viscosity. For trapping polystyrene beads, individual solvents like H_2O, MeOH and EtOH are good solvents and they are also miscible among each other.[68] We report our findings for a 90:10 volume mixture of H_2O–EtOH and H_2O–MeOH. When the volume of alcohol in water–alcohol binary mixtures increases beyond 10%, the viscosity of water–alcohol mixture increases rapidly until an equal volume mixture is reached.[69] Higher viscosity results in lower corner frequency. Thus, the corner frequency shift due to the temperature rise will be small, which will decrease the experimental signal to noise ratio.

4. Conclusions

In this work, based on a non-invasive 780 nm femtosecond optical trap, we have demonstrated the control and measurement of direct *in situ* temperature at the solid–liquid interface, induced by a co-propagating 1560 nm pulsed laser. The viscosity
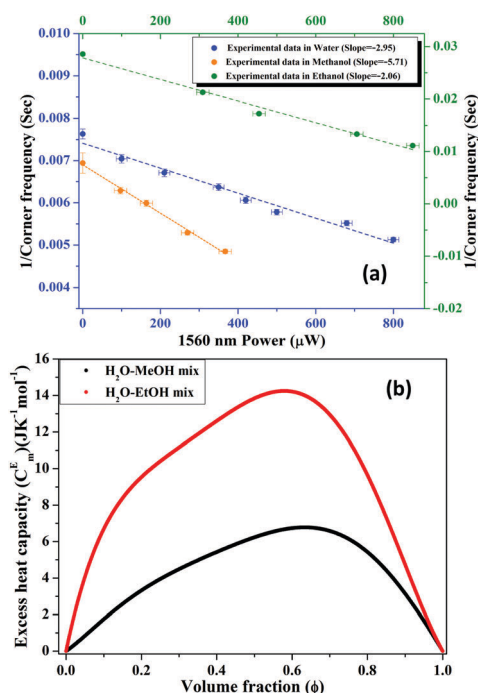
25828 | *Phys. Chem. Chem. Phys.*, 2016, **18**, 25823–25830

This journal is © the Owner Societies 2016

as well as temperature around the trapped bead has been measured from the changes in corner frequency values. These measurements show that the thermal energy of solvents is transformed into the kinetic energy of the trapped bead. Correspondingly, we have developed a theoretical model that can explain these experimental results. Last but not the least, we were also able to probe the intermolecular interaction between two closely behaving solvent molecules.

Acknowledgements

References

1 A. Ashkin, J. M. Dziedzic, J. E. Bjorkhom and S. Chu, *Opt. Lett.*, 1986, **11**, 288–290.

2 A. Ashkin, *Optical Trapping and Manipulation of Neutral Particles Using Lasers: A Reprint Volume with Commentaries*, World Scientific, 2006.

3 Q. Xing, F. Mao, L. Chai and Q. Wang, *Opt. Laser Technol.*, 2004, **36**, 635–639.

4 B. Agate, C. T. A. Brown, W. Sibbett and K. Dholakia, *Opt. Express*, 2004, **12**, 3011–3017.

5 A. K. De, D. Roy, A. Dutta and D. Goswami, *Appl. Opt.*, 2009, **48**, G33–G37.

6 D. Roy, A. K. De and D. Goswami, *Appl. Opt.*, 2015, **54**, 7002–7006.

7 A. Schönle and S. W. Hell, *Opt. Lett.*, 1998, **23**, 325–327.

8 P. Kumar and D. Goswami, *J. Phys. Chem. C*, 2014, **118**, 14852–14859.

9 D. Mondal and D. Goswami, *Biomed. Opt. Express*, 2015, **6**, 3190–3196.

10 D. Mondal and D. Goswami, *J. Nanophotonics*, 2016, **10**, 026013.

11 A. Ashkin and J. M. Dziedzic, *Science*, 1987, **235**, 1517–1520.

12 S. M. Block, D. F. Blair and H. C. Berg, *Nature*, 1989, **338**, 514–518.

13 A. Ashkin and J. M. Dziedzic, *Proc. Natl. Acad. Sci. U. S. A.*, 1989, **86**, 7914–7918.

14 A. Ashkin, J. M. Dziedzic and T. Yamane, *Nature*, 1987, **330**, 769–771.

15 G. Herzberg, *Infrared and Raman Spectra*, D. Van Nostrand: Princeton, 1945.

16 C. L. Braun and S. N. Smirnov, *J. Chem. Educ.*, 1993, **70**, 612–614.

17 A. I. Bishop, T. A. Nieminen, N. R. Heckenberg and H. Rubinsztein-Dunlop, *Phys. Rev. Lett.*, 2004, **92**, 198104.

18 A. Pommella, V. Preziosi, S. Caserta, J. M. Cooper, S. Guido and M. Tassieri, *Langmuir*, 2013, **29**, 9224–9230.

19 M. Tassieri, F. D. Giudice, E. J. Robertson, N. Jain, B. Fries, R. Wilson, A. Glidle, F. Greco, P. A. Netti, P. L. Maffettone, T. Bicanic and J. M. Cooper, *Sci. Rep.*, 2015, **5**, 8831.

20 Y. M. Rhee and V. S. Pande, *J. Phys. Chem. B*, 2008, **112**, 6221–6227.

21 D. de Sancho, A. Sirur and R. B. Best, *Nat. Commun.*, 2014, **5**, 4307.

22 M. Guoa, Y. Xub and M. Gruebelea, *Proc. Natl. Acad. Sci. U. S. A.*, 2012, **109**, 17863–17867.

23 M. Karplus and J. A. Mccammon, *Nat. Struct. Mol. Biol.*, 2002, **9**, 646–652.

24 R. M. Daniel, M. E. Peterson, M. J. Danson, N. C. Price, S. M. Kelly, C. R. Monk, C. S. Weinberg, M. L. Oudshoorn and C. K. Lee, *Biochem. J.*, 2010, **425**, 353–360.

25 M. L. Begasse, M. Leaver, F. Vazquez, S. W. Grill and A. A. Hyman, *Cell Rep.*, 2015, **10**, 647–653.

26 G. E. Uhlenbeck and L. S. Ornstein, *Phys. Rev.*, 1930, **36**, 823–841.

27 M. C. Wang and G. E. Uhlenbeck, *Rev. Mod. Phys.*, 1945, **17**, 323–342.

28 A. Einstein, *Ann. Phys.*, 1905, **322**, 549–560.

29 F. Reif, *Fundamentals of statistical and thermal physics*, McGraw-Hill, Sydney, 1965.

30 T. G. Mason, K. Ganesan, J. H. van Zanten, D. Wirtz and S. C. Kuo, *Phys. Rev. Lett.*, 1997, **97**, 3282–3285.

31 F. C. MacKintosha and C. F. Schmidt, *Curr. Opin. Colloid Interface Sci.*, 1999, **4**, 300–307.

32 M. Atakhorrami, J. I. Sulkowska, K. M. Addas, G. H. Koenderink, J. X. Tang, A. J. Levine, F. C. MacKintosh and C. F. Schmidt, *Phys. Rev. E: Stat., Nonlinear, Soft Matter Phys.*, 2006, **73**, 061501.

33 A. Yao, M. Tassieri, M. Padgett and J. Cooper, *Lab Chip*, 2009, **9**, 2568–2575.

34 T. Kalwarczyk, N. Zie-bacz, A. Bielejewska, E. Zaboklicka, K. Koynov, J. Szymanski, A. Wilk, A. Patkowski, J. Gapinski, H.-J. Butt and R. Hozyst, *Nano Lett.*, 2011, **11**, 2157–2163.

35 G. Charras and E. Sahai, *Nat. Rev. Mol. Cell Biol.*, 2014, **15**, 813–824.

36 Y. Pang and R. Gordon, *Nano Lett.*, 2012, **12**, 402–406.

37 D. Mondal and D. Goswami, *SPIE Proc.*, 2015, **9548**, 95481N.

38 P. Kumar, A. Khan and D. Goswami, *Chem. Phys.*, 2014, **441**, 5–10.

39 J. H. Lienhard IV and J. H. Lienhard V, *A Heat Transfer Textbook*, Phlogiston Press, Cambridge, Massachusetts, USA, 3rd edn, 2004.

40 Y. Liu, G. J. Sonek, M. W. Berns and B. J. Tromberg, *Biophys. J.*, 1996, **71**, 2158–2167.

41 H. S. M. Coxeter and S. L. Greitzer, *Geometry Revisited*, The Mathematical Association of America, Washington, DC, 1967.

42 http://www.olympus-ims.com/en/microscope/terms/luminous_flux/(accessed 14 July, 2016).

43 X. E. Lin, in Proceedings of the 1999 Particle Accelerator Conference, (IEEE, 1999), 1429–1431.

44 T. A. Scott, *J. Phys. Chem.*, 1946, **50**, 406–412.

45 J. Ortega, *J. Chem. Eng. Data*, 1982, **27**, 312–317.

46 J.-P. E. Grolier, *Fluid Phase Equilibrium*, 1981, **6**, 283–287.

47 G. C. Benson, P. J. D'Arcy and O. K. Kiyohara, *J. Solution Chem.*, 1980, **9**, 931–938.

48 J. D. Raal and R. L. Rijsdijk, *J. Chem. Eng. Data*, 1981, **26**, 351–359.

49 T. Al-Shemmeri, *Engineering Fluid Mechnanics*, Ventus Publishing ApS, 2012.

50 Dartmund Data Bank (DDB), http://ddbonline.ddbst.de/VogelCalculation/VogelCalculationCGI.exe.

51 J. Kendall and K. P. Monroe, *J. Am. Chem. Soc.*, 1917, **39**, 1787–1802.

52 M. Schnell and B. A. Wolf, *J. Rheol.*, 2000, **44**, 617–628.

53 R. Mertsch and B. A. Wolf, *Ber. Bunsenges. Phys. Chem.*, 1994, **98**, 1275–1280.

54 S. N. Damask, *Polarization Optics in Telecommunications*, Springer-Verlag, New York, 2005.

55 R. Radünz, D. Rings, K. Kroy and F. Cichos, *J. Phys. Chem. A*, 2009, **115**, 1674–1677.

56 D. Rings, R. Schachoff, M. Selmke, F. Cichos and K. Kroy, *Phys. Rev. Lett.*, 2010, **105**, 090604.

57 L. Joly, S. Merabia and J.-L. Barrat, *Europhys. Lett.*, 2011, **94**, 50007.

58 A. C. Richardson, S. N. S. Reihani and L. B. Oddershede, *Opt. Express*, 2008, **16**, 15709–15717.

59 R. Kubo, M. Toda and N. Hashitsume, *Statistical Physics*, Springer, Heidelberg, 1985, vol. 2.

60 W. H. Press, B. P. Flannery, S. A. Teukolsky and W. T. Vetterling, *Numerical Recipes. The Art of Scientific Computing*, Cambridge University Press, Cambridge, ch. 12.0, 1998.

61 K. Berg-Sørensen and H. Flyvbjerg, *Rev. Sci. Instrum.*, 2004, **75**, 594–612.

62 G. Pesce, A. Sasso and S. Fusco, *Rev. Sci. Instrum.*, 2005, **76**, 115105.

63 S. F. Tolić-Nørrelykkea, E. Schäffer, J. Howard, F. S. Pavone, F. Jülicher and H. Flyvbjerg, *Rev. Sci. Instrum.*, 2006, 77, 103101.

64 I.-M. Tolić-Nørrelykkea, K. Berg-Sørensen and H. Flyvbjerg, *Comput. Phys. Commun.*, 2004, **159**, 225–240.

65 H. Mao, J. R. Arias-Gonzalez, S. B. Smith, I. Tinoco, Jr. and C. Bustamante, *Biophys. J.*, 2005, **89**, 1308–1316.

66 A. Marcano, C. Loper and N. Melikechi, *J. Opt. Soc. Am. B*, 2002, **19**, 119–124.

67 G. C. Benson, P. J. D'Arcy and O. Kiyohara, *J. Solution Chem.*, 1980, **9**, 931–938.

68 D. Mukherji, C. M. Marques and K. Kremer, *Nat. Commun.*, 2014, **5**, 4882.

69 E. J. W. Wensink, A. C. Hoffmann, P. J. van Maaren and D. van der Spoel, *J. Chem. Phys.*, 2003, **119**, 7308–7317.

25830 | *Phys. Chem. Chem. Phys.*, 2016, **18**, 25823–25830

This journal is © the Owner Societies 2016